Collective and Individual Plasmon Resonances in Nanoparticle Films Obtained by Spin-Assisted Layer-by-Layer Assembly

Chaoyang Jiang, Sergiy Markutsya, and Vladimir V. Tsukruk*

Department of Materials Science and Engineering, Iowa State University, Ames, Iowa 50011

Received August 16, 2003. In Final Form: November 15, 2003

Nanoscale uniform films containing gold nanoparticle and polyelectrolyte multilayer structures were fabricated by the using spin-assembly or spin-assisted layer-by-layer (SA-LbL) deposition technique. These SA-LbL films with a general formula $[Au/(PAH-PSS)_nPAH]_m$ possessed a well-organized microstructure with uniform surface morphology and high surface quality at a large scale (tens of micrometers across). Plasmon resonance peaks from isolated nanoparticles and interparticle interactions were revealed in the UV−visible extinction spectra of the SA-LbL films. All films showed the strong extinction peak in the region of 510−550 nm, which is due to the plasmon resonance of the individual gold nanoparticles red-shifted because of a local dielectric environment. For films with sufficient density of gold nanoparticles within the layers, the second strong peak was consistently observed between 620 and 660 nm, which is the collective plasmon resonance from *intralayer* interparticle coupling. Finally, we suggested that, for certain film designs, *interlayer* interparticle resonance might be revealed as an independent contribution at 800 nm in UV−visible spectra. The observation of independent and concurrent individual, intralayer, and interlayer plasmon resonances can be critical for sensing applications, which involve monitoring of optomechanical properties of ultrathin optically active compliant membranes.

Introduction

Gold nanoparticles with a diameter from 1 to 100 nm are widely investigated as attractive candidates for inorganic−organic assemblies because of their unique optical and electronic properties.[1−3] These assemblies could find potential applications in advanced spectroscopy, chemical and biosensor technology, and microelectronic devices.[4−10] For example, surface-enhanced Raman scattering (SERS) is a highly sensitive spectroscopy that can detect individual molecules adsorbed on gold particles.[11] The SERS effect mainly comes from the enhancement of the local electromagnetic field near the surface, which is due to the excitation of the surface plasmon.[12] Systematically changing the geometry of a dielectric core−metal shell nanoparticle, it is possible to have a precisely controlled SERS effect.[13]

It has been shown that, by varying the particle shape, size, and spacing, the surface plasmon resonance (SPR) peak can be tuned in a wide range of wavelengths.[14] On the other hand, changing the environment and the level of the nanoparticles aggregation (distance and locations) can significantly affect the optical properties of matrix−nanoparticle composites or core−shell assemblies.[4,15,16] Thus, embedding the gold nanoparticles into organic−inorganic assemblies can be used to either tune their optical properties or measure optomechanical properties under external stimuli.[17−19] To date, several nanofabrication techniques have been applied for the construction of the gold nanoparticle−organic films including the most widely used Langmuir−Blodgett deposition,[20,21] chemical self-assembly,[22] and electrostatic layer-by-layer (LbL) assembly.[19] Those techniques provided organized molecular films with regular multilayered structures from a variety of polymeric and organic molecules.[23−27] The gold

* To whom correspondence should be addressed. E-mail: vladimir@iastate.edu.

(1) Hayat, M. A., Ed. *Colloidal Gold: Principles, Methods, and Applications*; Academic Press: San Diego, 1989; Vol. 1.
(2) Raschke, G.; Kowarik, S.; Franzl, T.; Sönnichsen, C.; Klar, T. A.; Feldmann, J.; Nichtl, A.; Kürzinger, K. *Nano Lett.* **2003**, *3*, 935.
(3) Krasteva, N.; Besnard, I.; Guse, B.; Bauer, R. E.; Mullen, K.; Yasuda, A.; Vossmeyer, T. *Nano Lett.* **2002**, *2*, 551.
(4) Fendler, J. H. *Chem. Mater.* **2001**, *13*, 3196.
(5) Nath, N.; Chilkoti, A. *J. Am. Chem. Soc.* **2001**, *123*, 8197.
(6) Mirkin, C. A. *Inorg. Chem.* **2000**, *39*, 2258.
(7) Sershen, S. R.; Westcott, S. L.; Halas, N. J.; West, J. L. *Appl. Phys. Lett.* **2002**, *80*, 4609.
(8) Cao, Y.; Jin, R.; Mirkin, C. A. *J. Am. Chem. Soc.* **2001**, *123*, 7961.
(9) Wang, Z.; Sasaki, T.; Muramatsu, M.; Ebina, Y.; Tanaka, T.; Wang, L.; Watanabe, M. *Chem. Mater.* **2003**, *15*, 807.
(10) Morris, T.; Copeland, H.; McLinden, E.; Wilson, S.; Szulczewski, G. *Langmuir* **2002**, *18*, 7261.
(11) Chang, R. K., Furtak, T. E., Eds. *Surface-Enhanced Raman Scattering*; Plenum: New York, 1982.
(12) Chen, C. Y.; Burstein, E. *Phys. Rev. Lett.* **1980**, *45*, 1287.
(13) Jackson, J. B.; Westcott, S. L.; Hirsch, L. R.; West, J. L.; Halas, N. J. *Appl. Phys. Lett.* **2003**, *82*, 257.
(14) Félidj, N.; Aubard, J.; Lévi, G.; Krenn, J. R.; Salerno, M.; Schider, G.; Lamprech, B.; Leitner, L. A.; Aussenegg, F. R. *Phys. Rev. B* **2002**, *65*, 075419.
(15) Hutter, E.; Fendler, J. H.; Roy, D. *J. Phys. Chem. B* **2001**, *105*, 11159.
(16) Caruso, F.; Spasova, M.; Salgueiriño-Maceira, V.; Liz-Marzán, L. *Adv. Mater.* **2001**, *13*, 1090. Westcott, S. L.; Oldenburg, S. J.; Lee, T. R.; Halas, N. J. *Langmuir* **1998**, *14*, 5396. Gittins, D. I.; Caruso, F. *J. Phys. Chem. B* **2001**, *105*, 6846.
(17) Schmitt, J.; Decher, G.; Dressick, W. J.; Brandow, S. L.; Geer, R. E.; Shashidhar, R.; Calvert, J. M. *Adv. Mater.* **1997**, *9*, 61.
(18) Sershen, S. R.; Westcott, S. L.; West, J. L.; Halas, N. J. *Appl. Phys. B* **2001**, *73*, 379.
(19) Fu, Y.; Xu, H.; Bai, S.; Qiu, D.; Sun, J.; Wang, Z.; Zhang, X. *Macromol. Rapid Commun.* **2002**, *23*, 256.
(20) Chen, S. *Langmuir* **2001**, *17*, 2878.
(21) Huang, S.; Tsutsui, G.; Sakaue, H.; Shingubara, S.; Takahagi, T. *J. Vac. Sci. Technol., B* **2001**, *19*, 2045.
(22) Wang, B.; Wang, H.; Li, H.; Zeng, C.; Hou, J. G.; Xiao, X. *Phys. Rev. B* **2000**, *63*, 035403.
(23) Ulman, A. *Introduction to Ultrathin Organic Films*; Academic Press: San Diego, 1991.
(24) Tsukruk, V. V. *Prog. Polym. Sci.* **1997**, *22*, 247. Tsukruk, V. V.; Rinderspacher, F.; Bliznyuk, V. N. *Langmuir* **1997**, *13*, 2171. Bliznyuk, V. N.; Rinderspacher, F.; Tsukruk, V. V. *Polymer* **1998**, *39*, 5249. Tsukruk, V. V. *Adv. Mater.* **2001**, *13*, 95.
(25) Decher, G. *Science* **1997**, *277*, 1232. Lvov, Y.; Ariga, K.; Ichinose, I.; Kunitake, T. *J. Am. Chem. Soc.* **1995**, *117*, 6117. Lvov, Y.; Decher, G.; Mohwald, H. *Langmuir* **1993**, *9*, 481. Decher, G.; Lvov, Y.; Schmitt, J. *Thin Solid Films* **1994**, *244*, 772. Lvov, Y.; Decher, D. *Crystallogr. Rep. (Transl. Kristallografiya)* **1994**, *39*, 628.

10.1021/la0355085 CCC: $27.50
Published on Web 12/30/2003

nanoparticle−polyelectrolyte multilayer superlattices with tunable optical properties have been fabricated with the LbL technique.[17] In these condensed, organized films, the gold nanoparticles embedded in an organic matrix with very different dielectric properties are subject to strong interaction with this matrix and with each other within and between individual layers. These interactions generate collective plasmon resonances, which are caused by the interaction between neighboring gold particles controlled by the long-range aggregation of the gold nanoparticles within the same layer.[28] A variable packing density and, thus, interparticle distances along with a changing dielectric constant of interparticular media are considered to be major factors affecting the dipolar−dipolar interactions and SPR appearance.[29] A red shift of the SPR peak is usually expected and observed for inorganic nanoparticles embedded in an organic matrix. As a rule, only a single broad adsorption peak is detected for these assemblies without clear visible contributions from individual and collective resonances.[6,28,30−32] Very few studies considered this effect and demonstrated separated contributions from individual and collective SPRs for very well-defined structures such as those obtained with microlithography.[14,28]

In this work, we discuss our results on the fabrication of LbL-assembled multilayered films containing gold nanoparticles in an aggregation state controlled by the design of the multilayered films with various combinations of polymer interlayers. We focus on studies of their microstructure and corresponding SPR optical response. Careful design of these multilayers revealed superimposed but separated SPR peaks caused by individual resonances from the gold nanoparticles and collective resonances originating from intralayer interparticle interactions.

Experimental Section

Reagents and Materials. The polymer for LbL assembly, namely, poly(ethylene imine) (PEI, MW = 25 000), poly(allylamine hydrochloride) (PAH, MW = 65 000), and poly(sodium 4-styrenesulfonate) (PSS, MW = 70 000) were purchased from Aldrich and used without further purification. Ultrapure water with a resistivity of 18 MΩ·cm used in all experiments was purified with a Nanopure system. Quartz substrates were cleaned with a fresh Royal solution [1:3 (v/v) HNO_3/HCl]. Silicon wafers cut to a typical size of 10 × 20 mm were cleaned in a piranha solution [1:3 (v/v) H_2SO_4/H_2O_2], according to a usual procedure adapted in our laboratory.[33] *Attention: royal and piranha solutions are extremely dangerous and should be very carefully treated.* Silicon wafers of the {100} orientation with one side polished (Semiconductor Processing Co.) and quartz plates with both sides polished (Chemglass Co.) were atomically smooth. After cleaning, the substrates were then rinsed thoroughly with Nanopure water and dried with dry nitrogen before they were used.

Fabrication of Gold Nanoparticles/LbL Multilayers. Gold nanoparticles of different diameters from 2 to 25 nm were prepared according to the known procedure described in the literature.[34,35] Small-sized particles were synthesized by using thiocyanate as a reducing agent, while larger nanoparticles were obtained by using sodium citrate. For example, particles with a 12.7-nm diameter used throughout this study were synthesized as follows: 5 mL of a 1% sodium citrate solution was quickly injected into 50 mL of a boiling 1 mM $HAuCl_4$ solution. The solution was kept under boiling conditions for 10 min and continuously stirred for an additional 15 min. Gold nanoparticle solutions were stored at room temperature in a dark area and used within 3 weeks. Sodium citrate left in the solution after the synthesis of gold particles surrounds the gold nanoparticles so that they are quite stable in solution. These nanoparticles bear a modest negative charge under normal pH conditions.[16,36]

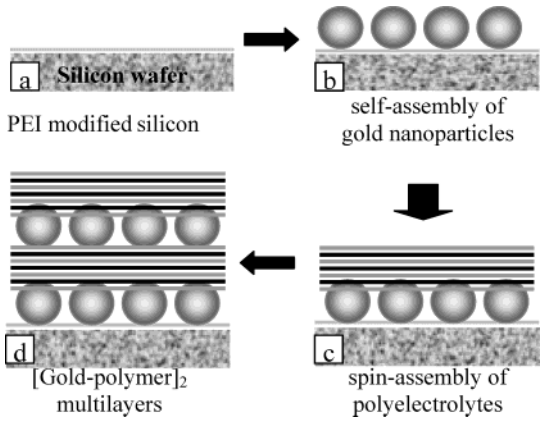

Figure 1. Scheme of fabrication of gold nanoparticle−polyelectrolyte multilayers: (a) assembly of a PEI monolayer on a silicon wafer; (b) gold nanoparticle monolayer deposited by adsorption on the PEI surface; (c) Au/(PAH−PSS)$_n$PAH multilayers fabricated with SA-LBL assembly of polyelectrolyte layers; and (d) assembly of the [Au/(PAH−PSS)$_n$PAH]$_2$ multilayer structure.

For initial modification of the silicon surface, freshly cleaned substrates were first immersed in a 1% PEI solution for 15 min to form a polyelectrolyte monolayer with a thickness of about 1 nm. After activation with HCl solution, the slightly positively charged substrates were immersed in a gold nanoparticle solution for a certain time period ranging from 1 to 30 min to facilitate electrostatically driven adsorption. Then, the substrates were rinsed with pure water to remove the loosely tethered particles.

The multilayered films with different thicknesses were fabricated by the spin-assembly or spin-assisted LbL (SA-LbL) method, which is a combination of spin coating and conventional LbL techniques. The SA-LbL technique has been recently introduced as a time- and cost-efficient assembly and successfully applied to a range of polyelectrolytes and nanoparticles.[37,38] The thickness of the deposited layers can be controlled by solvent evaporation, spin speed, spin time, and solute concentration.[39] We applied SA-LbL to construct polymer multilayers and nanoparticle-containing layers with a low density of nanoparticles. However, conventional LbL was exploited to deposit high-density nanoparticle interlayers. This way, we fabricated [Au/(PAH−PSS)$_n$PAH]$_m$ films as presented in Figure 1. According to usual LbL terminology, n (ranging from 0 to 15) corresponded to the number of polymer bilayers and m (ranging from 1 to 3) corresponded to the number of gold nanoparticle/polymer bilayers. Polyelectrolytes were dissolved in Nanopure water with 0.2% concentration. In the course of SA-LbL fabrication, a droplet of 150 μL of the polyelectrolyte solution was dropped on the silicon substrate and rotated for 20 s with a 3000-rpm rotation speed. The substrates were rinsed twice by Nanopure water and dried

(26) He, J.-A.; Valluzzi, R.; Yang, K.; Dolukhanyan, T.; Sung, C.; Kumar, J.; Tripathy, S. K.; Samuelson, L.; Balogh, L.; Tomalia, D. A. *Chem. Mater.* **1999**, *11*, 3268.
(27) Tsukruk, V. V.; Bliznyuk, V. N.; Visser, D. W.; Campbell, A. L.; Bunning, T.; Adams, W. W. *Macromolecules* **1997**, *30*, 6615.
(28) Rechberger, W.; Hohenau, A.; Leitner, A.; Krenn, J. R.; Lamprecht, B.; Aussenegg, F. R. *Opt. Commun.* **2003**, *220*, 137.
(29) Kuhn, H. In *Biophysik*; Hoppe, W., Lohmann, W., Markl, H., Ziegler, H., Eds.; Springer: Berlin, 1982; p 289.
(30) Mulvaney, P. *Langmuir* **1996**, *12*, 788.
(31) Sastry, M.; Gole, A.; Patil, V. *Thin Solid Films* **2001**, *384*, 125.
(32) Taleb, A.; Petit, C.; Pileni, M. P. *J. Phys. Chem. B* **1998**, *102*, 2214.
(33) Tsukruk, V. V.; Bliznyuk, V. N. *Langmuir* **1998**, *14*, 446.
(34) Grabar, K. C.; Freeman, R. G.; Hommer, M. B.; Natan, M. J. *Anal. Chem.* **1995**, *67*, 735.
(35) Johnson, S. R.; Evans, S. D.; Mahon, S. W.; Ulman, A. *Supramol. Sci.* **1997**, *4*, 329.
(36) Malikova, N.; Pastoriza-Santos, I.; Schierhorn, M.; Kotov, N. A.; Liz-Marzán, L. *Langmuir* **2002**, *18*, 3694.
(37) Cho, J.; Char, K.; Hong, J.-D.; Lee, K.-B. *Adv. Mater.* **2001**, *13*, 1076.
(38) Chiarelli, P. A.; Johal, M. S.; Casson, J. L.; Roberts, J. B.; Robinson, J. M.; Wang, H.-L. *Adv. Mater.* **2001**, *13*, 1167.
(39) Chiarelli, P. A.; Johal, M. S.; Holmes, D. J.; Casson, J. L.; Robinson, J. M.; Wang, H.-L. *Langmuir* **2002**, *18*, 168.

while spinning for 30 s. This procedure was repeated until a designed number of the bilayers *n* was achieved. All SA-LbL films were prepared in a class 100 clean room to avoid contamination and to ensure high optical quality of the films. A fabrication time of about 2 min per bilayer resulted in a very time-efficient procedure: films with 10−20 bilayers were fabricated within 20−40 min instead of the usual 5−10 h with manual or robotic arm routines.

The optical properties of the gold nanoparticle solutions and multilayered SA-LbL films on quartz substrates were measured with a Shimadzu 1601 UV−visible spectrometer. Structure characterization was conducted with atomic force microscopy (AFM). AFM topographical and phase images were collected with Dimension or Multimode AFM microscopes (Digital Instruments) in the tapping mode under ambient conditions in accordance with a usual procedure adapted in our laboratory.[40] Silicon tips with spring constants of 50 N/m were used for most scans. Tip radii were in the range of 20−40 nm as calculated from the profiles of a reference gold nanoparticle standard.[41] For selected high-resolution images, carbon nanotube tips with a tip radius of 5−11 nm (Nanodevices) were used. AFM images were obtained on different scales ranging from 500 nm to 50 μm with a scanning rate of 1 Hz. To obtain the surface microroughness, a 1 × 1 μm surface area was normally measured. A film thickness was routinely obtained from the bearing analysis of the surface areas with a scratch produced by a sharp steel needle. Independently, the thickness of the polymer multilayers was measured with a Compel Ellipsometer (InOmTech, Inc.). The average thickness of the SiO_2 layer was measured prior to the polymer deposition and used for the analysis of the ellipsometry data with a double-layer model.[42] The refractive indixes for polymers and silicon oxides were taken from literature.[43,44] However, it is worth noting that, as a result of the strong absorption, the thickness of the films with high-density gold particles cannot be obtained easily from ellipsometry measurement.

Results and Discussions

Monolayer of Gold Nanoparticles. From the analysis of the AFM images of the gold nanoparticles, the mean diameter was estimated from surface histograms constructed for at least 50−100 nanoparticles (Figure 2). After analyzing the size distribution and optical properties for several batches of gold nanoparticles with a diameter ranging from 2 to 25 nm, for further studies we selected the nanoparticles with the average diameter of 12.7 ± 1.3 nm (Figure 2c). The nanoparticle diameter and its variation (∼10%) were close to the results from Grabar et al.[34] This selection gave us nanoparticles of reasonable solution concentration, high storage lifetime, relatively narrow size distribution, and clear optical response.

The final concentration of gold in the solution was close to 1 mmol/L. Therefore, the aggregation number per particle was about 6 × 10^4 and the concentration of gold nanoparticles was about 1.5 × 10^{-8} mol/L assuming a complete reaction. The UV−visible spectra of these solutions displayed a strong plasmon resonance peak around 519 ± 0.5 nm caused by SPR of individual nanoparticles (Figure 2d).[45,46] This strong absorption gives the solution of gold nanoparticles its characteristic intense burgundy color.

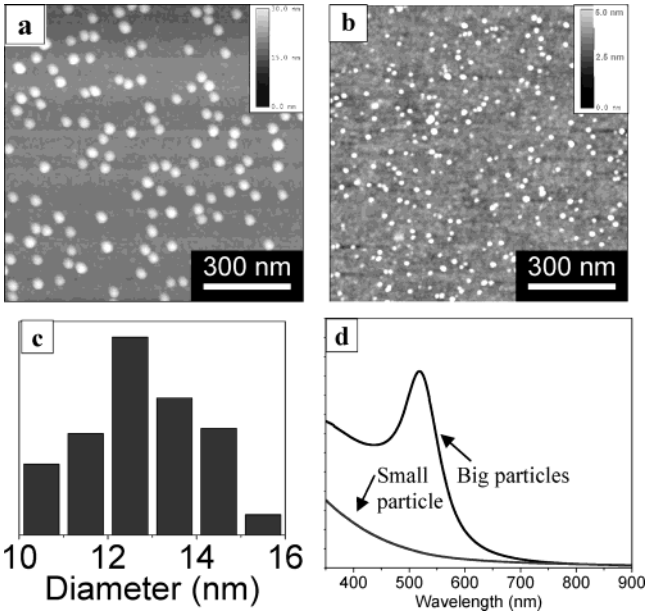

Figure 2. (a) AFM topographical image of well-separated larger gold nanoparticles diameter 12.7 ± 1.3 nm; (b) AFM topographical image of smaller gold nanoparticles, diameter 2.3 ± 1.2 nm; (c) height histogram of gold nanoparticles with the diameter of 12.7 ± 1.3 nm obtained from AFM data; (d) UV−visible extinction spectrum of larger and smaller gold nanoparticle solutions.

Gold nanoparticles are rarely adsorbed on a bare silicon surface because of unfavorable Coulombic interactions (both surfaces are slightly negatively charged): only 40−50 nanoparticles were found in the surface area of 10 × 10 μm. The modification of the silicon surface with a positively charged PEI monolayer resulted in efficient, electrostatically driven adsorption of gold nanoparticles: 1200 nanoparticles were found within 1 × 1 μm on the PEI surface. Additional surface activation by 0.01 mol/L HCl solution resulted in a significant increase of the surface coverage: 1800 gold nanoparticles were found within the 1 μm^2 surface area.

To control the gold nanoparticle density (surface coverage and interparticle distance) during the deposition, the assembly on the PEI monolayer was stopped by a "sudden dilute" technique and the substrate was then rinsed and dried. Increasing the deposition time resulted in the higher surface coverage increasing from 250 nanoparticles/μm^2 for a short deposition time up to a saturation limit of 1800 particles/μm^2. The concentration of the gold nanoparticles solution is the most important factor affecting the surface coverage (Figure 3). For the lowest surface coverage tested here, the mean distance between nanoparticles was about 88 nm, which exceeded their diameter manifold (distance/diameter ratio of 7:1). For the medium surface coverage of 5−10%, the interparticle distance decreased to 40−50 nm (distance/diameter ratio of 4:1). Finally, at the saturation level, a virtually "complete monolayer" of gold nanoparticles became visible on the AFM images (Figure 3c,d). Large-scale AFM images showed a smooth, high-quality surface with microroughness below 5 nm and the absence of microscopic bumps originating from external contaminations. However, this smooth surface morphology at a high magnification represented a common AFM artifact associated with tip dilation of the lateral dimensions of nanoscale objects.[47] Misleading AFM images of

(40) Tsukruk, V. V.; Reneker, D. H. *Polymer* **1995**, *36*, 1791. Tsukruk, V. V. *Rubber Chem. Technol.* **1997**, *70*, 430. Ratner, B., Tsukruk, V. V., Eds. *Scanning Probe Microscopy of Polymers*; ACS Symposium Series; American Chemical Society: Washington, D.C., 1998; Vol. 694.
(41) Vesenka, J.; Manne, S.; Giberson, R.; Marsh, T.; Henderson, E. *Biophys. J.* **1993**, *65*, 992.
(42) Azzam, R. M. A.; Bashara, N. M. *Ellipsometry and Polarized Light*; North-Holland Pub. Co.: Amsterdam, New York, 1977.
(43) Aranishi, Y.; Takahashi, H. *Jpn. Kokai Tokkyo Koho* **2000**, 6.
(44) Van Krevelen, D. W. *Properties of Polymers*; Elsevier: Amsterdam, 1997.
(45) Bohren, C. F.; Huffman, D. R. *Absorption and Scattering of Light by Small Particles*; John Wiley and Sons: New York, 1983.
(46) Kreibig, U.; Vollmer, M. *Optical Properties of Metal Clusters*; Springer Press: Berlin, 1995.
(47) Magonov, S.; Whangbo, M.-H. *Surface Analysis with STM and AFM*; VCH: Weinheim, 1996.

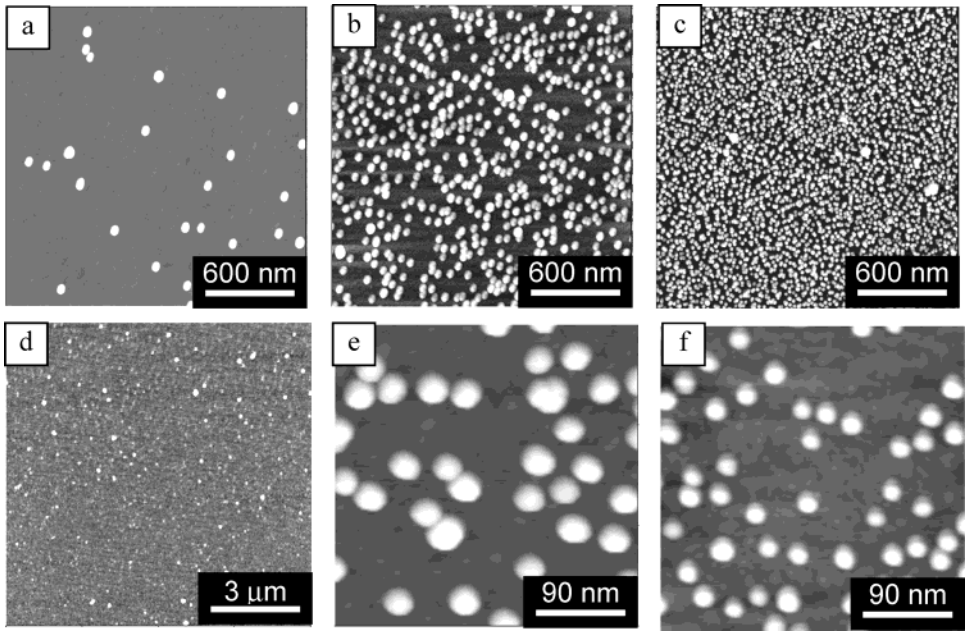

Figure 3. AFM topographical images of the gold nanoparticle monolayer with different surface coverages fabricated by using different concentrations of solution, *z* scale is 30 nm: (a) the lowest surface coverage obtained from a 1.5×10^{-10} mol/L solution; (b) low surface coverage of 2% obtained from a 1.5×10^{-9} mol/L solution; (c) the highest surface coverage of 22% obtained from a 1.5×10^{-8} mol/L solution; (d) larger scale area of the same sample as that in part c; and (e and f) high-resolution topographical image of gold nanoparticles with a surface coverage of 8% obtained with a conventional silicon tip (e) and carbon nanotube tip (f). The appearance of nanoparticles is affected by the tip dilation, which is sensitive to a low point between the particles reachable by the tip.

"complete" monolayers should be treated with great care. This effect is demonstrated in Figure 3e,f, displaying two high-resolution AFM images of the gold nanoparticles obtained with an ordinary silicon tip and a carbon nanotube tip. The dilation effect was much smaller (but still present) on the AFM image obtained with the nanotube tip that allowed the evaluation of the nanoparticle concentration for the highest surface coverage. This corresponded to the surface coverage of 22% and the average interparticle distance of 26 nm or the 2:1 distance/diameter ratio. This distance falls in the range where effective collective SPR between neighboring nanoparticles is expected. Achieving a higher surface concentration under these conditions was prevented by repulsive interactions among nanoparticles. This value was relatively high considering that the maximum achievable surface coverage that produces a 1:1 distance/diameter ratio for different symmetries of particles is within 75−91% and the percolation limit for spherical particles is close to 55%.[48] These parameters can only be reached for lightly charged nanoparticles.[4]

Figure 4 shows the UV−visible extinction spectra of gold nanoparticle monolayers with different surface coverages. Unlike the spectrum for the solution in Figure 2, two broad peaks were observed in the region of 500−700 nm. These peaks could be clearly separated after background subtraction and fitting with Lorentzian functions, as demonstrated for one spectrum in Figure 4. The strong and sharp extinction peak, which appeared around 518 ± 0.5 nm with the width of 53 nm, was virtually unchanged for all monolayers and was caused by the plasmon resonance of isolated gold nanoparticles similarly to that of dilute solutions. The height of this peak showed almost a linear increase with the increase of the surface density.

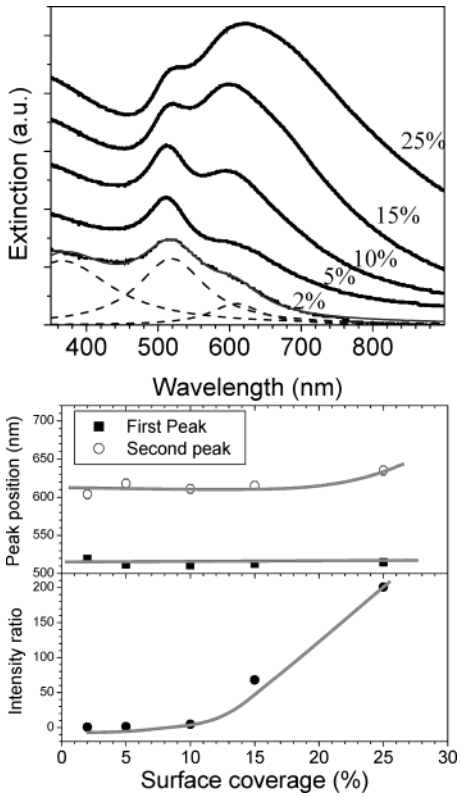

Figure 4. Top: UV−visible extinction spectra of gold nanoparticle monolayers with different surface coverages. Bottom: the variation of positions of two resonance bands and their intensity ratio (the intensity of the second to first plasmon peak).

Another broad peak appeared around 615 nm at a low surface concentration and was red-shifted to 635 nm for the highest surface coverage (Figure 4). The appearance of this second peak is associated with interparticle

(48) Karim, A.; Tsukruk, V. V.; Douglas, J. F.; Satija, S. K.; Fetters, L. J.; Reneker, D. H.; Foster, M. D. *J. Phys. II* **1995**, *5*, 1441.

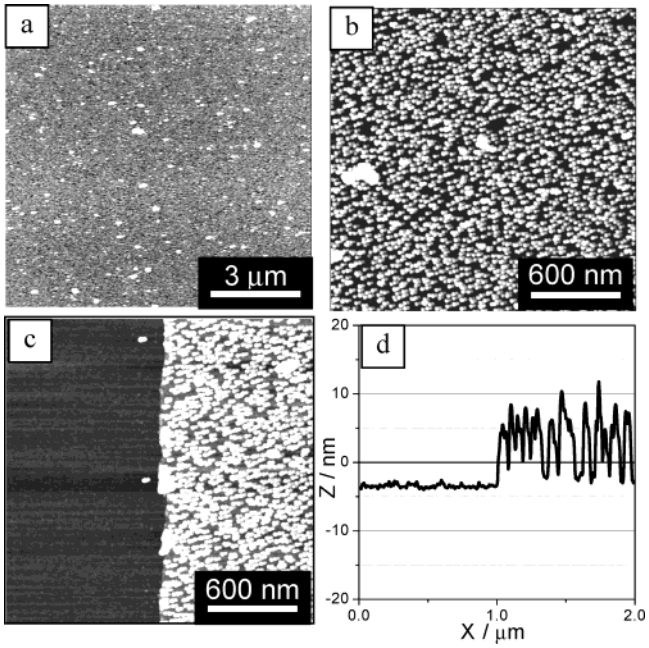

Figure 5. AFM topography image and line scan profile of Au/(PAH−PSS)PAH multilayered films: (a) large-scale AFM image; (b) higher-resolution AFM image; (c) AFM image of the film edge, *Z* scale is 30 nm; and (d) cross section of image c.

resonances, which strongly depend on the distance/diameter ratio, among other factors.[14,28,49,50] The absorption at this wavelength was very minor for the low surface coverage when the distance/diameter ratio was relatively high (4:1 to 7:1) and increased dramatically for the higher surface coverage. It became predominant (integral intensity is 200 higher for the second peak than for the first peak) for the 22% surface coverage when the distance/diameter ratio decreased to 2:1. In fact, such a shape was predicted for a pair of nanoparticles when the distance/diameter ratio falls below 2:1, but it is not usually observed because of the low surface coverage achieved experimentally.[17,50] We observed a dominance of collective plasmon resonance for monolayers with the distance/diameter ratio below 3:1 (Figure 4).

Because of insufficient surface coverage and nonuniformity of interparticle distance distribution in a vast majority of experiments, only a gradual red shifting of a broad peak is usually observed without separation of collective and individual resonances.[17] In contrast, our experiments clearly indicated that this broad peak was not originated from the red shift of the individual particle plasmon peak but had a composite nature and contained both individual and collective plasmon resonances.[50,51] The collective surface plasmon band depends strongly on interparticle separation and, thus, is sensitive to the chemical environment of the particle and its interaction with its surroundings.[36,50,52] As shown in the following, nanoparticle-containing multilayers with a sufficiently small interparticle distance produced a strong appearance of the distinctive collective resonance peak, which was sensitive to changing the interparticle distance of gold nanoparticles within intra- and interlayered structures.

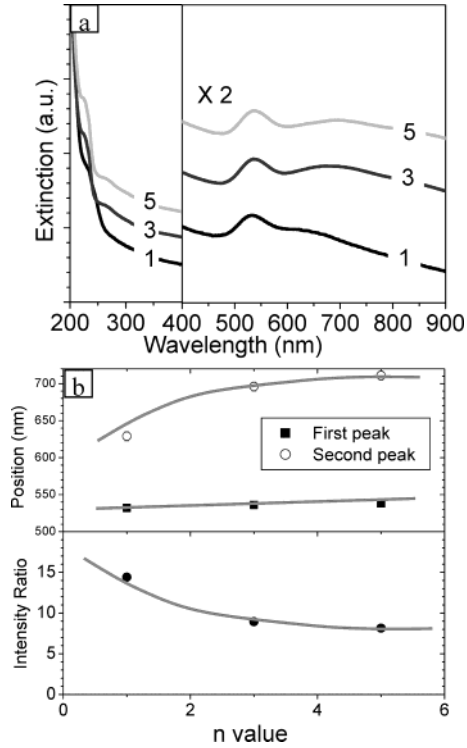

Figure 6. (a) UV−visible extinction spectra of Au/(PAH−PSS)$_n$PAH multilayers, with *n* of 1, 3, and 5, respectively. Gold nanoparticle surface coverage is 5%. (b) The variation of plasmon resonance peak positions and their intensity ratio (the intensity of the second to first plasmon peak).

Gold Nanoparticle−Polymer Multilayer Films. The fabrication of the multilayered films began with the deposition of a first polymer bilayer on top of the gold nanoparticle monolayer (Figure 1). Figure 5 shows the AFM images of a gold nanoparticle array with a PAH−PSS bilayer spin-assembled on top. A large-scale AFM image (10 × 10 μm) showed uniformity of this film with the overall microroughness not exceeding 2.5 nm. The higher-resolution AFM image of the same layer, Au/(PAH−PSS)PAH, showed a surface coverage similar to that measured before spin assembly of the top polymer layers. This indicated that the gold nanoparticles were strongly attached to the surface of the PEI monolayer and were not dissolved or washed away during the spin coating and spin rinsing.

The surface of the Au/(PAH−PSS)PAH film was relatively rough as a result of incomplete surface coverage with gold nanoparticles as indicated by significant surface microroughness. As can be seen from the line scan across the scratched film, the gold nanoparticles were covered by a PAH−PSS bilayer, resulting in a total thickness of nanoparticle aggregates of about 15 nm (the diameter of 12.7 nm + 2.3 nm of the PAH−PSS bilayer; Figure 5). The PAH−PSS bilayer thickness of 2.7 nm was independently obtained from the film areas without gold nanoparticles. The surface microroughness decreased with an additional deposition of the polymer bilayers. Indeed, for the sample Au/(PAH−PSS)$_{10}$PAH, where 10 bilayers were deposited, the multilayer film was very smooth with the microroughness well below 2 nm.

UV−visible spectra of Au/(PAH−PSS)$_n$PAH multilayers measured for 5% surface coverage of gold nanoparticles revealed virtually constant intensity of the red-shifted first peak appearing around 535 nm with exact positions of 532 ± 0.5, 536 ± 0.5, and 538 ± 0.5 nm for Au/(PAH−PSS)$_n$PAH with *n* equal to 1, 3, and 5, respectively (Figure

(49) Jensen, T. R.; Malinsky, M. D.; Haynes, C. L.; Van Duyne, R. P. *J. Phys. Chem. B* **2000**, *104*, 10549.
(50) Schmitt, J.; Mächtle, P.; Eck, D.; Möhwald, H.; Helm, C. A. *Langmuir* **1999**, *15*, 3256.
(51) Westcott, S. L.; Oldenburg, S. J.; Lee, T. R.; Halas, N. J. *Chem. Phys. Lett.* **1999**, *300*, 651.
(52) Ung, T.; Liz-Marzán, L. M.; Mulvaney, P. *J. Phys. Chem. B* **2001**, *105*, 3441.

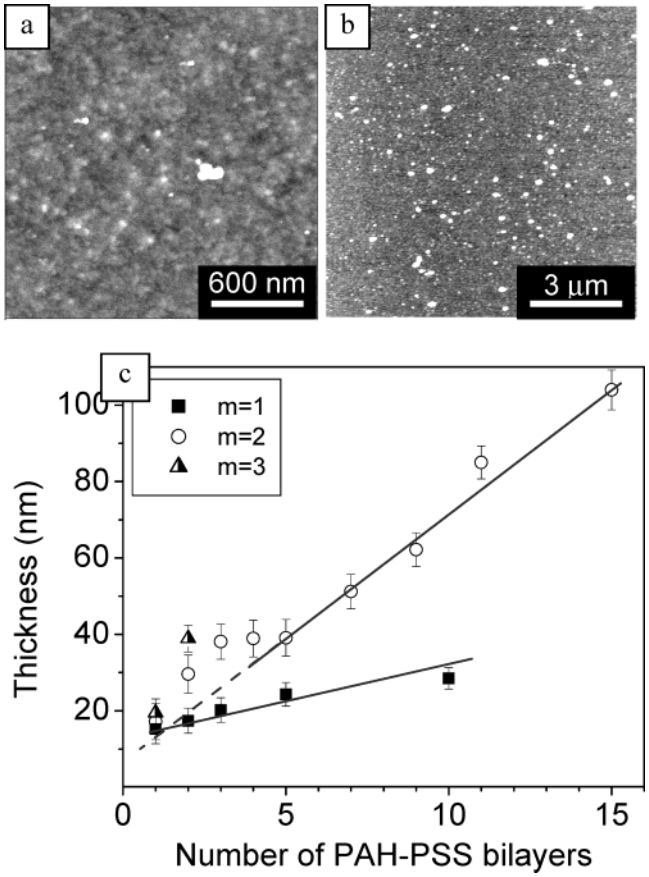

Figure 7. AFM topographical images of the [Au/(PAH−PSS)$_5$PAH]$_2$ film, *z* scale is 30 nm: (a) higher-resolution image; (b) large-scale image; and (c) the variation of the film thickness for [Au/(PAH−PSS)$_n$PAH]$_m$ for different combinations of *n* and *m*. Two data points for $m = 3$ are presented for illustrative purposes.

6). These peaks were 13−20-nm red-shifted compared to the gold nanoparticle solution (519 nm). This red shift was usually observed for the gold nanoparticles coated with a polymer layer or dissolved in different solvents and is caused by changing the dielectric environment.[53,54] For a matrix with a large refractive index, the position of the surface plasmon band would shift to a longer wavelength.[30] With increasing the bilayer number, thicker films covering the gold nanoparticle resulted in the further red shift of the adsorption peak. It should be noted that the second peak for the Au/(PAH−PSS)$_n$PAH multilayers changed similarly (Figure 6). With a larger number of polymer layers deposited on the gold nanoparticles, the intensity increased and the peak was further red-shifted. This can also be explained by the changing interparticle interaction because of the added dielectric layers. However, collective resonance was much more sensitive to the environment composition because red shifting was more pronounced with the position changing from 630 to 720 nm (Figure 6). Finally, a strong absorption peak appearing around 225 nm was caused by the contribution from the PSS chains and was used here for the independent control of polymer layer deposition.[37] The linear increase of that peak with the number of deposited layers was another strong evidence of the multilayer fabrication despite sparse arrangement of the gold nanoparticles.

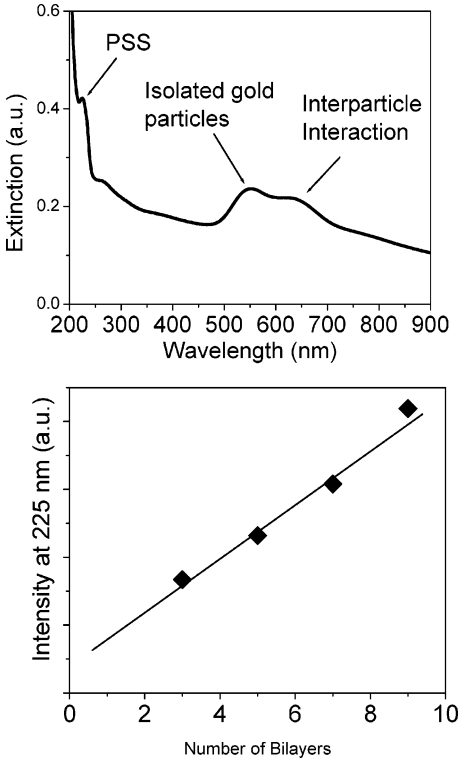

Figure 8. Top: UV−visible extinction spectrum of the [Au/(PAH−PSS)$_n$PAH]$_2$ film with 22% gold nanoparticle surface density with three major adsorption bands marked. Bottom: a linear increase of the absorption at 225 nm with the bilayer number *n*.

As a next step, we fabricated multilayered films containing two and three gold layers designed as presented in Figure 1. Both large-scale and higher-resolution AFM topography images of [Au/(PAH−PSS)$_5$PAH]$_2$ films with a high density of gold nanoparticles possessed a microroughness of 4 nm within 1 × 1 μm surface areas and a film thickness of 40 nm. The thickness of the multilayered films [Au/(PAH−PSS)$_n$PAH]$_m$ changed linearly with the number of polymer bilayers for different combinations of gold nanoparticles and polymer layers for larger *n* (Figure 7). Deviations from linear behavior observed for a small number of bilayers can be explained by partially filling the polyelectrolyte into the empty space between the gold nanoparticles. The linear increase is a strong evidence of the formation of the multilayered structure in the films. The slope of the thickness dependence upon a number of polymer bilayers gives the average PAH−PSS bilayer thickness of 3.2 nm in the [Au/(PAH−PSS)$_n$PAH]$_2$ film for larger *n*. This value is close to the estimated thickness of the first bilayer (2.7 nm as discussed previously) and corresponds to the results of ellipsometry measurement of (PAH−PSS)$_n$ multilayers, which were spin-assembled without gold nanoparticles.[25]

The UV−visible spectrum of the gold nanoparticle−polymer films with a high density of gold nanoparticles (22% surface coverage) is shown in Figure 8. Three clear peaks can be obviously observed for the [Au/(PAH−PSS)$_n$PAH]$_2$ film. The peak at 225 nm showed a linear increase of the PSS material with increasing number of deposited bilayers (Figure 8). The intensity of strong plasmon resonance of individual nanoparticles at 540 nm was twice that for [Au/(PAH−PSS)$_n$PAH] films with a single gold nanoparticle layer, which indicates good reproducibility in the deposition of the second gold-containing layer. The strong collective resonance peak

(53) Mayya, K. S.; Schoeler, B.; Caruso, F. *Adv. Funct. Mater.* **2003**, *13*, 183.
(54) Huang, S.; Minami, K.; Sakaue, H.; Shigubara, S.; Takahagi, T. *J. Appl. Phys.* **2002**, *92*, 7486.

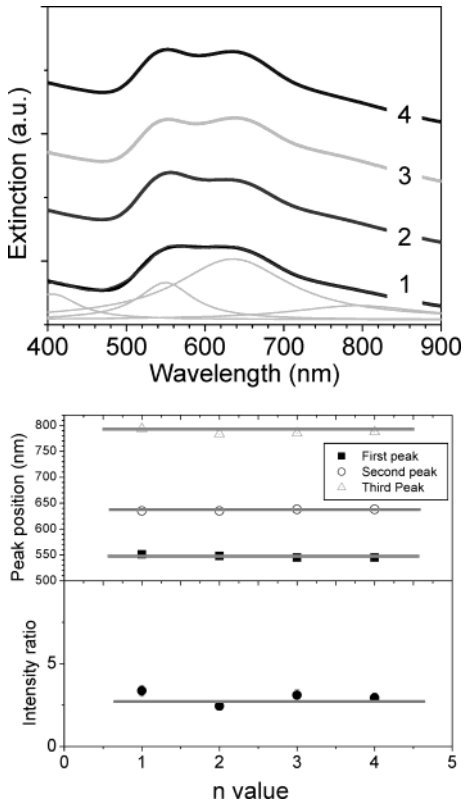

Figure 9. Top: UV−visible extinction spectra of [Au/(PAH−PSS)$_n$PAH]$_2$ films with high gold nanoparticle density (22% surface coverage), with n equal to 1, 2, 3, and 4. These spectra can be fitted with three Lorentzian peaks, as shown for $n = 1$. Bottom: the variation of the plasmon resonance peak positions and the intensity ratio (the intensity of the second to first plasmon peak).

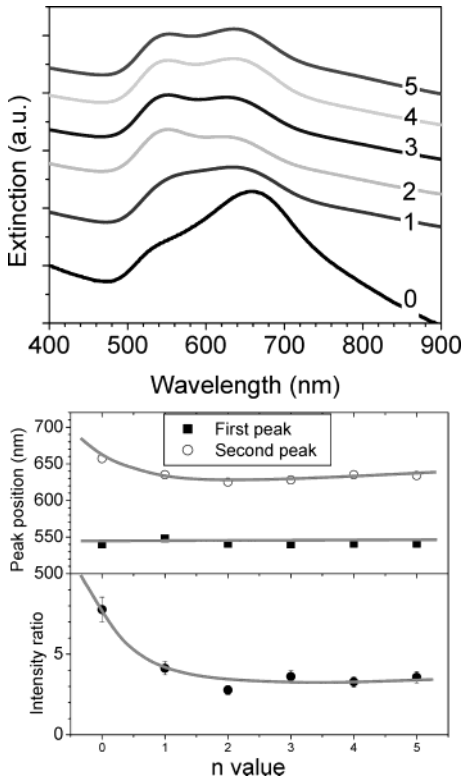

Figure 10. Top: UV−visible extinction spectra of [Au/(PAH−PSS)$_n$PAH]$_2$ films with medium gold nanoparticle density (15% surface coverage), with n equal to 0, 1, 2, 3, 4, and 5. Bottom: the variation of the plasmon resonance peak positions and their intensity ratio (the intensity of the second to first plasmon peak).

appeared at 640 nm. This peak was also observed for gold nanoparticle monolayers and was associated with interparticle interactions within the layer (*intralayer resonance*). One can expect that an additional contribution associated with additional interactions between the gold nanoparticles located in adjacent layers (*interlayer resonance*) can be detected for some multilayer combinations. To the best of our knowledge, such a separate contribution was not experimentally observed for such small nanoparticles probably as a result of the masking by very strong intralayer resonance. Thus, we fabricated a series of multilayers with an increasing number of polymer bilayers between gold intralayers to ensure different intra- and interlayer spacings that can be instructive in the separation of inter- and intralayer resonance contributions.

The UV spectra of the [Au/(PAH−PSS)$_n$PAH]$_2$ multilayers with two layers containing 22% gold nanoparticle separated by the polymer interlayer with different thicknesses (n varied from 1 to 4, which corresponds to the thickness changing from 3.3 to 13.5 nm) showed two clear major peaks with a significant long-wavelength contribution around 800 nm that appeared during fitting analysis (Figure 9). Similar results were obtained for films containing three gold nanoparticle layers [Au/(PAH−PSS)$_n$PAH]$_3$. A plasmon band of isolated gold nanoparticles in these films was further red-shifted as a result of the presence of additional polymer layers and appeared around 548 nm. The collective plasmon resonance peak appeared in the range of 630−640 nm, as was observed before. This peak is very broad with a long-lasting right shoulder (Figure 9).

Similar spectra were observed for the [Au/(PAH−PSS)$_n$-PAH]$_2$ film with a lower concentration of gold nanoparticles (Figure 10). For the film with a single polymer layer between the two gold nanolayers ($n = 0$), we observed a very strong plasmon peak at 656 nm with its intensity 8 times higher than the intensity of individual plasmon resonance. Increasing the separation between gold-containing nanolayers caused decreasing intensity and a blue shift of this peak (Figure 10). The position of this maximum and its intensity became similar to that observed for the gold nanoparticle monolayer only when the distance between layers increased above the distance/diameter ratio of 2:1.

To clarify this behavior and verify the nature of observed long-wave resonance, several new [Au/(PAH−PSS)$_n$PAH]$_2$ films with gold layers separated by three polymer layers (about 7-nm thick) were prepared by using solutions with different concentrations of gold nanoparticles (Figure 11). Indeed, only an individual plasmon peak was observed for the multilayers with an average intralayer distance/diameter ratio between 4:1 and 7:1. Obviously the very low overall concentration of gold nanoparticles was not sufficient to generate any collective resonances. For multilayers with a higher concentration of gold nanoparticles (distance/diameter ratio of 3:1 and lower), an additional contribution in the range of 600−660 nm showed up with a clearly separated second, red-shifted peak appearing for a gold nanoparticle content of 15% and higher (distance/diameter ratio of 2.5:1 and 2:1; Figure 11). The optical data obtained for selected [Au/(PAH−PSS)$_n$PAH]$_3$ films followed the general trends described previously.

However, what is more important is the clear appearance of a long-wavelength contribution for a higher con-

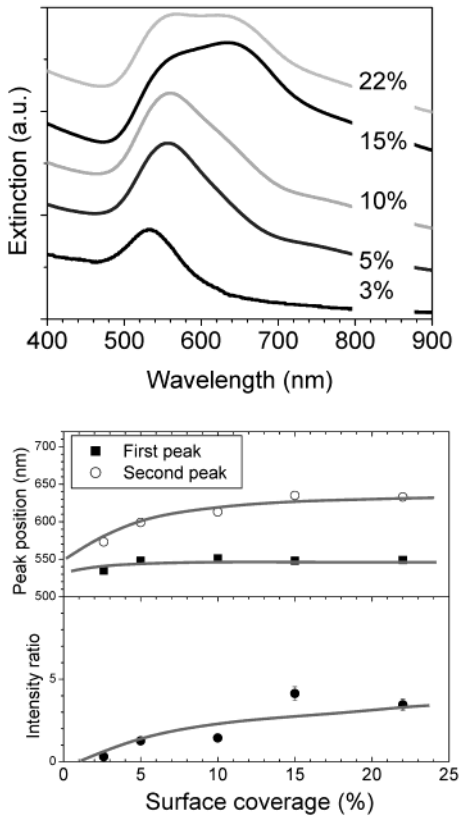

Figure 11. Top: UV−visible extinction spectra of $[Au/(PAH-PSS)_nPAH]_2$ films with different gold nanoparticle densities. Bottom: the variation of the plasmon resonance peak positions and their intensity ratio (the intensity of the second to first plasmon peak).

centration of gold nanoparticles, which showed up as a wide peak at 780−790 nm similarly to that which appeared on the fitting result in Figure 9 (Figures 9−11). The maximum contribution of this additional peak (reaching up to 40% of the integral intensity) was revealed for the multilayered film with two polymer bilayers between gold layers. This contribution decreased for both smaller and larger separations of gold layers to below 20% of the integral intensity, suggesting that the optimized interlayer distance of about 6 nm is required to enhance the appearance of interlayer resonance for the films studied here. These changes (intensity and maximum position), directly related to the variation of the interlayer spacing while the intralayer spacing remains unchanged, directly suggest the presence of a strong contribution from interparticle resonances *between gold nanolayers* in addition to the intralayer resonance discussed previously. This phenomenon confirms the suggestion made previously on the presence of the independent contribution originating from collective resonance between gold nanoparticles, which belong to different interlayers in the multilayer films (*interlayer collective resonances*) in addition to the usually observed *intralayer collective resonances*.

Film Microstructure and Optical Properties. The results on optical properties presented previously can be understood considering the real microstructure of gold multilayers derived from AFM data. The sketch of the $[Au/(PAH-PSS)_nPAH]_2$ film with the distance/diameter ratio of 2:1 is presented in Figure 12. The formation of bilayered gold films with incomplete surface coverage and a small number of polymer bilayers between inevitably goes through a stage of "filling" the "empty" space available within the first deposited gold nanoparticle monolayer. In this case, the polymer layers form shells around gold nanoparticles with the thickness controlled by a number of bilayers in the manner presented in Figure 12. The estimated total thickness of the two-layer gold nanoparticle film with three polymer layers between them and parameters obtained from experimental data is about 32 nm, which is fairly close to the experimental result of 38 nm (Figure 7).

For this microstructure, the distance/diameter ratio is determined by the equation $1 + nL/D$, where L is the thickness of a polymer layer and D is the diameter of the gold nanoparticles. Considering that, for a small number of layers, the thickness of the individual polymer layer is about 1.4 nm, we can estimate the distance/diameter ratio for this microstructure to be close to 1.3:1. For this ratio, a strong collective resonance contribution in the range of 800 nm was both predicted theoretically and observed experimentally for metal nanoparticles with larger diameters.[28,55] In thicker films, a gradual increase of the separation between gold-containing layers causes an increasing distance/diameter ratio to values close to the intralayer values and, thus, gradual disappearance of this contribution for thicker films. It is obvious that achieving a higher nanoparticle density and reaching its theoretical percolation limit of 55% for two-dimensional systems of short-range ordered spherical objects[56,57] should result in

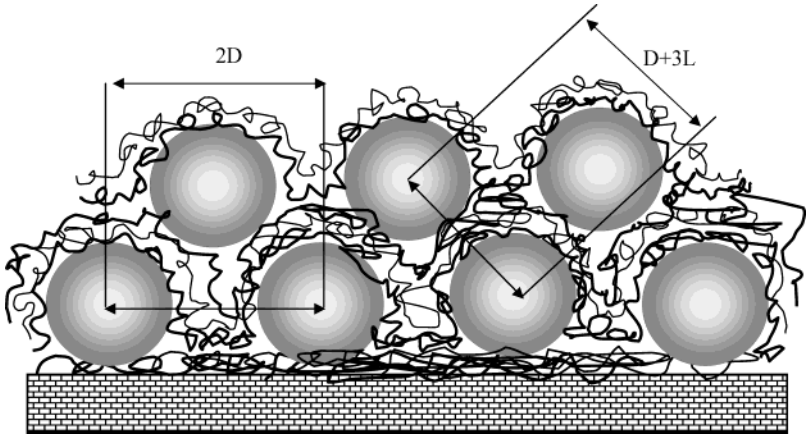

Figure 12. Microstructure of the film composed of two gold nanoparticle layers separated by three polymer layers, $[Au/(PAH-PSS)_1PAH]_2$, demonstrating different distance/diameter ratios for intralayer and interlayer distances and used for the estimation of the total film thickness. It shows that for incomplete gold nanoparticle layers the thickness of the film with two gold nanoparticle layers is below a doubled value for a single layer.

a much stronger interlayer collective resonance contribution and clear separation of intralayer and interlayer contributions, which is the subject of the current investigation. Such a phenomenon, if achieved, can be critical for optomechanical sensing applications of gold-containing multilayer films that rely on the detection of changes of local intralayer and interlayer microstructures.

Conclusions

In summary, organized multilayer films from gold nanoparticles and polyelectrolyte multilayers have been fabricated very time efficiently with LbL and SA-LbL assembly techniques. SA-LbL films $[Au/(PAH-PSS)_nPAH]_m$ with different designs possessed a well-organized microstructure with uniform surface morphology and high optical quality. All SA-LbL films showed the strong extinction peak in the range of 510−550 nm, which is due to the plasmon resonance of the individual gold nanoparticles red-shifted because of a local dielectric environment. For films with sufficient gold nanoparticle density within the layers (10−22%), the second strong peak was consistently observed between 620 and 660 nm, which is due to the collective plasmon resonance from *intralayer* interparticle coupling. Finally, we suggested that, under certain conditions, *interlayer* interparticle resonance could be separated as an additional, independent contribution around 800 nm in UV−visible spectra. This observation was obtained for multilayer films with a conventional level of the dense surface coverage (that is, within 10−20% surface coverage). The independent and concurrent detection of all individual, intralayer, and interlayer plasmon resonances for carefully designed multilayered films with a higher content of gold nanoparticles achievable with LbL assembly can be critical for sensing applications that involve monitoring of optomechanical properties of these optically active films. A first example of a robust, high-sensitive, free-suspended film of this type has been recently demonstrated.[58]

Acknowledgment. We thank S. Peleshanko and M. Ornatska for useful discussions. This work is supported by the NSF, CTS-0210005 Grant, AFOSR, F496200210205 Grant, NASA, NAG 102098 Contract, and Department of Commerce, M01-C03 Grant, through The National Textile Center.

LA0355085

(55) Lal, S.; Westcott, S. L.; Taylor, R. N.; Jackson, J. B.; Nordlander, P.; Halas, N. J. *J. Phys. Chem. B* **2002**, *106*, 5609.
(56) Kooij, E. S.; Brouwer, E. A. M.; Wormeester, H.; Poelsema, B. *Langmuir* **2002**, *18*, 7677.
(57) Yu, A.; Liang, Z.; Cho, J.; Caruso, F. *Nano Lett.* **2003**, *3*, 1203.
(58) Jiang, C.; Markutsya, S.; Tsukruk, V. V. *Adv. Mater.*, accepted for publication.